WPMST1-CPR(18) 20676

F Nespoli et al.

Application of a two-fluid two-point model to SolEdge2D-EIRENE modeling of TCV H-mode plasmas

Preprint of Paper to be submitted for publication in Proceeding of 23rd International Conference on Plasma Surface Interactions in Controlled Fusion Devices (PSI-23)

This work has been carried out within the framework of the EUROfusion Consortium and has received funding from the Euratom research and training programme 2014-2018 under grant agreement No 633053. The views and opinions expressed herein do not necessarily reflect those of the European Commission.

Application of a two-fluid two-point model to SolEdge2D-EIRENE simulations of TCV H-mode plasmas

F. Nespoli[1], H. Bufferand[2], M. Valentinuzzi[2], N. Fedorczak[2], G. Ciraolo[2], E. Serre[1], R. Maurizio[3],H. De Oliveira[3], B. Labit[3], M. Komm[4], M. Faitsch[5], S. Elmore[6], The TCV team[7], The EUROfusion MST1 team[8]

[1] *Aix Marseille Univ, CNRS, Centrale Marseille, M2P2, Marseille, France*
[2] *IRFM, CEA Cadarache, F-13108 St. Paul-lez-Durance, France*
[3] *École Polytechnique Fédérale de Lausanne (EPFL), Swiss Plasma Center (SPC), 1015 Lausanne, Switzerland*
[4] *Institute of Plasma Physics AS CR, Za Slovankou 3, 182 00 Prague 8, Czech Republic*
[5] *Max-Planck-Institute for Plasma Physics, Boltzmannstr. 2, D-85748 Garching, Germany*
[6] *CCFE, Culham Science Center, Abingdon, OX14 3DB, United Kingdom*
[7] *see author list of S.Coda et al., Nucl. Fusion 57 (2017) 102011*
[8] *see author list of H. Meyer et al., Nuclear Fusion 57 (2017) 102014*
Email: federico.nespoli@univ-amu.fr

Abstract

The edge and scrape-off layer (SOL) plasma of the inter-ELM phase of an H-mode discharge from the TCV tokamak is modeled with the transport code SolEdge2D-EIRENE [H. Bufferand et al, Nuclear Fusion 55 (2015)] The numerical simulations, in presence and in absence of C impurities sputtered from the first wall, are presented and compared with the experiments, finding an overall good agreement. The application of the standard two-point model to the simulation results leads to an apparent momentum gain along the divertor leg. A two-fluid two-point model featuring thermally decoupled ions and electrons is introduced and applied to the simulation results, overcoming this apparent discrepancy.

---

1 Introduction

The influence of the divertor leg length L_{div} on the heat loads at the divertor plates has been recently investigated in the TCV tokamak [1] L-mode plasmas, finding a spreading of the SOL heath flux decay length λ_q for increasing L_{div}, believed to be due to active turbulence along the divertor leg [2, 3]. Ongoing experiments in TCV are performed within the medium-size Tokamak (MST) task force of the EUROfusion consortium to extend this previous study to H-mode plasmas. The SolEdge2D-EIRENE code [4] is used in support of the experimental campaign to help the interpretation of the results. This is a state-of-the art transport code, featuring a realistic description of both the plasma magnetic geometry and of the first wall, including pumps and gas puff locations. The transport dynamics of all the ionization states of impurities is also included in the code [5].
The two-point model [6] is a powerful interpretative and predictive tool, which can be applied to both experimental and simulation results, providing the relationship between upstream plasma parameters (electron density and temperature n_e, T_e) and the values at the target plate (i.e. at the divertor). Though, it is based on several assumptions, as for example the ion and electron temperature being equal $T_i = T_e$, and its application to simulation or experimental results can sometimes give misleading results such as an apparent momentum gain in the divertor [7]. Some improvement to the two-point model [8, 9] are therefore sometimes needed to avoid misinterpreting the results.

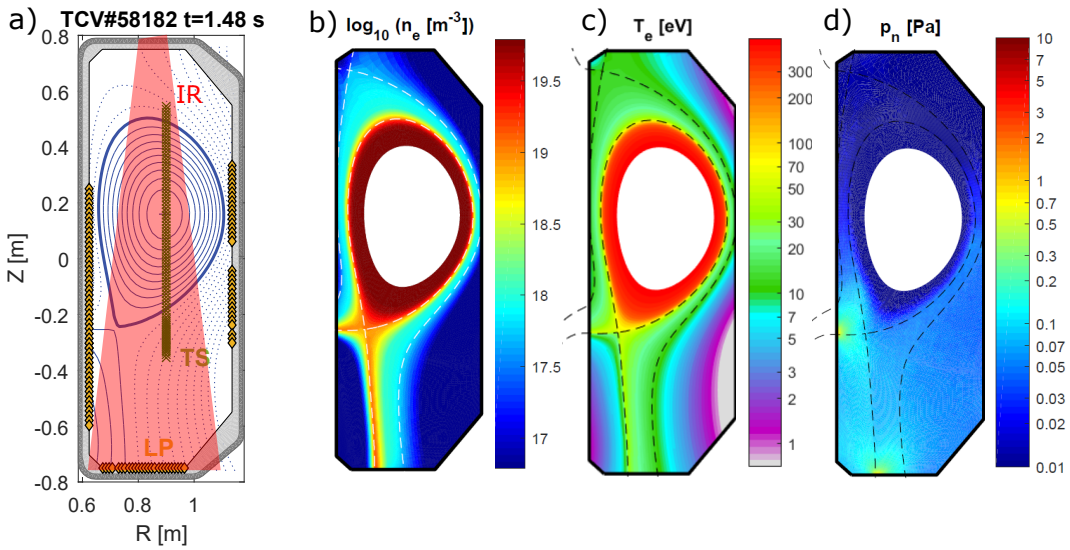

Figure 1: a) Magnetic equilibrium reconstruction from TCV#58182, together with the location of TS measurements (green crosses), LP (orange diamonds) and the IR field of view (red). Results from the SolEdge2D-EIRENE simulation of b) electron density n_e c) electron temperature T_e d) neutral pressure p_n.

2 Modeling of TCV H-mode inter-ELM phase

We consider the TCV discharge #58182. This is an H-mode plasma with 0.2 MW of Neutral Beam Heating power, featuring a long divertor leg, being the vertical position of the magnetic axis $Z_{ax} = +12$ cm, with plasma current $I_p = 380$ kA and average electron density $n_{e,av} = 6 \cdot 10^{19}\mathrm{m}^{-3}$. The magnetic equilibrium, reconstructed from the LIUQE code [10], is shown in Fig. 1 together with the location of the main diagnostics used in the experiment: the electron density and temperature n_e, T_e of the main plasma are measured by means of Thomson Scattering (TS); at the divertor plates, n_e and T_e are measured by Langmuir Probes (LP) with the methodology detailed in Ref. [11], and the inter-ELM parallel heat flux $q_{||}$ is extracted by means of InfraRed thermography (IR) [3].

The SolEdge2D-EIRENE grid is built on the magnetic equilibrium shown in Fig.1. In order to correctly reproduce the pedestal, the transport coefficients D and χ are allowed to vary in the radial direction. Their local value is determined through an automatic feedback procedure on radial profiles of n_e and T_e deduced by inter-ELM TS measurements. Inside the Last Closed Flux Surface (LCFS) $T_i = T_e$ is assumed, while $T_i > T_e$ in the SOL. D and χ are assumed to be poloidally constant, and the recycling coefficient for Deuterium (D) at the wall is $R = 0.99$. A snapshot of the simulation results of n_e, T_e and the neutral pressure p_n is shown in Fig. 1b-d. A second simulation including carbon (C) impurities sputtered from the wall (recycling coefficient for C $R = 0.5$) is performed.

In Fig. 2a,b we compare the electron temperature T_e and density n_e as measured by TS (black points) with the simulated radial profiles of temperature and density from the simulations. In particular, the electron temperature and density are shown in blue, while the ion temperature and density are shown in red; the results from the simulation with deuterium (D) are shown with dashed lines, while the ones from the simulation featuring carbon impurities (D+C) are shown with solid lines. In both cases the agreement with the experimental data is satisfactory. In the D+C case the impurities cool the SOL lowering slightly T_e. Due to the inclusion of C, the electron density is

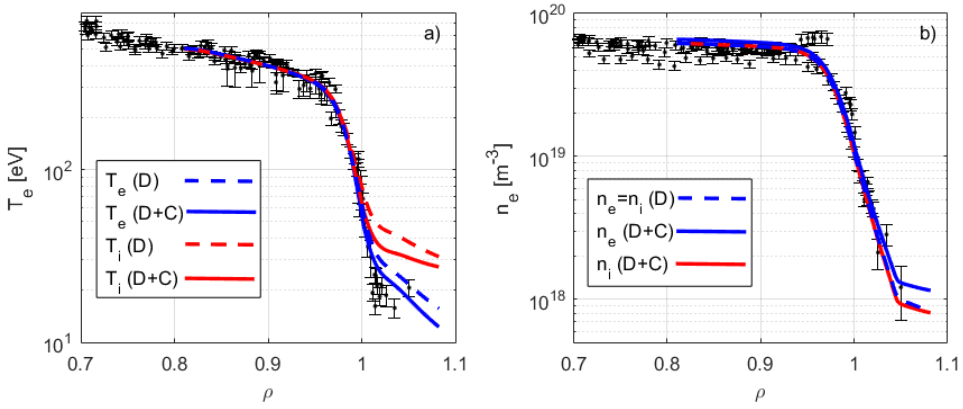

Figure 2: a) TS measurements of electron temperature T_e (black points) compared with the T_e (blue) and T_i (red) profiles at the outer midplane from the simulation in deuterium (dashed line), and with sputtered carbon (solid lines). b) TS measurements of electron density n_e (black points) compared with the n_e (blue) and n_i (red) profiles at the outer midplane from the simulation in deuterium (dashed line, $n_i = n_e$ not shown), and with sputtered carbon (solid lines).

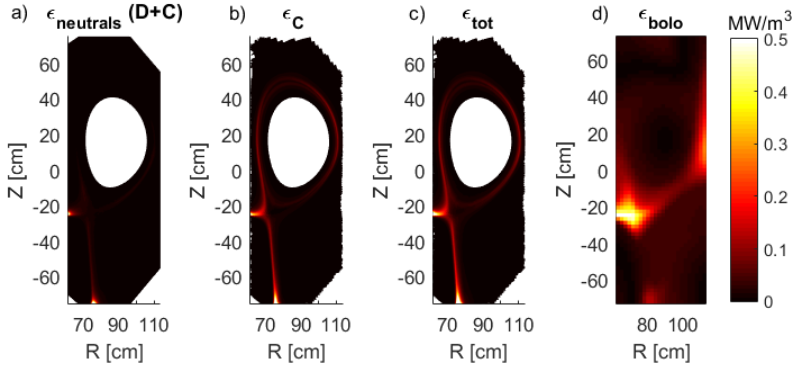

Figure 3: Simulated emissivity ϵ due to a) neutrals (D+C) b) line radiation from ionized C. c) Total simulated ϵ. d) Experimental ϵ from tomographic inversion of 64 line-integrated bolometric measurements. The color coding is the same for all plots.

slightly increased, with a maximum relative variation (still modest) in the SOL.
The 2D distribution in the poloidal cross-section of radiated emissivity ϵ is shown in Fig. 3 for the D+C simulation. The total emissivity (Fig. 3c), concentrated around the separatrix with peaks at the strike points, is dominated by line radiation from ionized carbon (Fig. 3b), while the radiation from neutrals (Fig. 3a) becomes important only in front of the strike points. The experimentally measured emissivity, resulting from the inversion of 64 line-integrated bolometric measurements, is shown in Fig. 3d. Simulated and measured emissivity qualitatively agree, both exhibiting a hollow profile with ϵ peaked around the LCFS and the strike points. Though, experimentally ϵ is also peaked in the X-point region, while this feature is not captured by the simulations.
Finally, in Fig.4 we compare the simulated profiles (orange lines) of ion saturation current density j_{sat}, electron temperature T_e and parallel heat flux $q_{||}$ measured from both LP (blue dots) and IR thermography (solid black line). The radial profiles of these quantities are plotted against the radial upstream coordinate r_u, being $r_u = 0$ at the LCFS. The profiles measured by LP and IR exhibit a radial shift towards smaller major radius R, the peak occuring inside the private flux

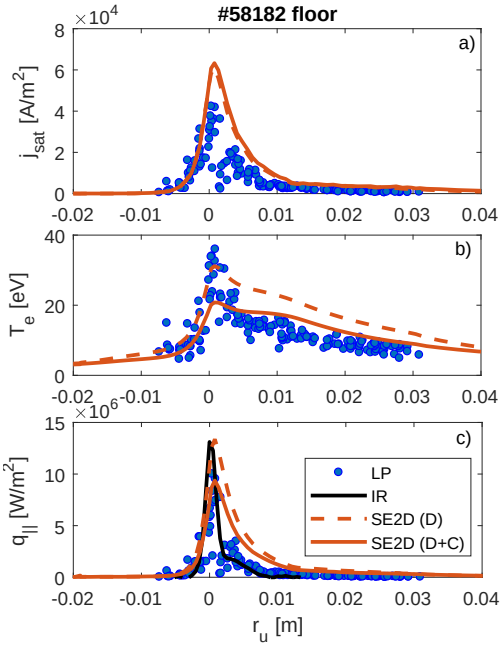

Figure 4: Radial profiles of a) ion saturation current density j_{sat} b) electron temperature T_e and c) parallel heat flux $q_{||}$ measured from both LP (blue dots) and IR thermography (solid black line), measured at the outer strike point and remapped upstream. The profiles of the same quantities from the simulations in the D (dashed lines) and D+C (solid lines) cases are also shown.

region. This is most probably due to an error in the magnetic reconstruction, being less precise at the strike point. Therefore, in Fig.4 a corrective shift of $\Delta r_u = 1.5$ mm has been applied to the experimental profiles. As there is an overall agreement between the simulated quantities and the experimentally measured ones, we notice an overestimation of the simulated j_{sat} (or n_e) for both the D (dashed line) and D+C (solid line) cases. We remark that close to the separatrix j_{sat} (i.e. n_e) measured by LP could be underestimated due to the fact that the floating potential is strongly negative here $V_{fl} \sim -40$ V, preventing the probes to completely reach the ion saturation regime. T_e, also overestimated in the D case, is lowered by the power radiated from impurities in the D+C case, resulting in a better agreement with the experimental one. The parallel heat flux measured from LP (blue dots), $q_{||} = \gamma_{sh} n_e c_s T_e$ with $\gamma_{sh} = 7$ the sheath transmission factor, matches the one measured by IR thermography (black solid line). While for the D case (orange dashed line) the simulated peak value of $q_{||}$, $q_{||,peak}$ agrees with the experimental one, the total heat flux at the strike point is higher than in the experiments, being $q_{int,sim}/q_{int,exp} \sim 3$, with $q_{int} = \int q_{||}(r_u) dr_u$, consistently with the overestimation of both n_e and T_e. In the D+C case, $q_{||,peak}$ lowers accordingly to T_e, and the total heat flux gets closer to the experimental one $q_{int,sim}/q_{int,exp} \sim 2.2$. In general, the simulated profiles are substantially broader than the experimentally measured ones. This could be due to the lack of poloidal variation of the transport coefficients, assumed to vary only in the radial direction. Also, drifts are not included in the simulations; LP measurements show a sharp variation of the floating potential V_{fl} close to the separatrix, that could steepen the pressure profiles as obsreved for limited plasmas [12, 13, 14].

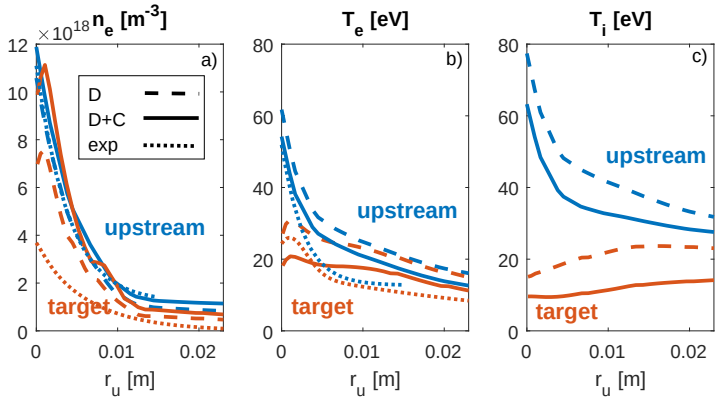

Figure 5: Radial upstream (blue) and target (orange) profiles in the SOL of a) electron density n_e b) electron temperature T_e c) ion temperature T_i, for both fit of experimental data from TS and LP (dotted lines) and simulations (dashed (D) and solid (D+C) lines).

3 Two-fluid two-point model

The two-point model [6] relates upstream and target quantities. It relies on the basic assumptions that, within a flux tube, the particle flux and the total plasma pressure $\Pi = 2k_b nT(1+M^2)$ (being M the mach number) are conserved, and that the heat is transported by parallel heat conductivity. By further assuming $M = 0$ upstream and the Bohm condition at the sheath entrance $M = 1$, the model is described by the following equations:

$$T_u^{7/2} = T_t^{7/2} + \frac{7L_{||} f_{cond} q_u}{2\kappa_{0,e}} \tag{1}$$

$$q_u = q_t/(1 - f_{power}) = \frac{n_t c_s \gamma_{sh} T_t}{1 - f_{power}} \tag{2}$$

$$2n_t T_t = f_{mom} n_u T_u \tag{3}$$

where n and T are the plasma density and temperature (assumed to be equal for ions and electrons), q is the parallel heat flux with the sheat transmission factor $\gamma_{sh} = 7$, $L_{||}$ is the parallel connection length between the upstream and the target location, $\kappa_{0,e} = (4\pi\epsilon_0)^2/\sqrt{(m_e)}\ln\Lambda e^4 Z \sim 1.3 \cdot 10^{69}$ [MKS units] is the electron heat conductivity. The corrective factors f_{power} and f_{mom} are the power and pressure loss respectively due to volumetric processes, while f_{cond} is the fraction of parallel power q_u carried by conduction, responsible for the formation of temperature gradients along the field lines. The subscripts u and t indicate upstream and target quantities, respectively, the former being identified in the following analysis with the outer midplane. By combining eqs.(1-2), we obtain

$$T_u^{7/2} = T_t^{7/2} + \frac{7L_{||} f_q n_t c_s \gamma_{sh} T_t}{2\kappa_{0,e}} \tag{4}$$

where we define the total power loss factor $f_q \equiv f_{cond}/(1 - f_{power})$, including both volumetric and convective losses. In Fig.5 we show the upstream and target profiles of n_e (a), T_e (b) and T_i (c) for both simulations (dashed (D) and solid (D+C) lines, same as in Fig. 2 and 4 for $r_u \geq 0$) and experiments (dotted lines). The experimental upstream profiles are obtained from TS measurements (Fig. 2), fitted with a modified hyperbolic tangent function following Ref. [15]. We remark that these data are quite poorly resolved outside the LCFS, especially in the far SOL (no measurements

for $r_u \geq 15$ mm). The target profiles are obtained from LP measurements (Fig. 4), exhibiting a different slope in the near and far SOL, are fitted with the function

$$f(x) = \sum_{i=1}^{2} \frac{f_{0,i}}{2} \exp\left[\left(\frac{S}{2\lambda_i}\right)^2 - \frac{x - x_0}{\lambda_i}\right] \operatorname{erfc}\left(\frac{S}{2\lambda_i} - \frac{x - x_0}{S}\right) \tag{5}$$

in order to better preserve the profile shape. This is a convolution of a double exponential decay (as observed in limited plasmas [16]) with a Gaussian accounting for diffusion in the private flux region, similarly to what originally done with a single exponential decay in the SOL [17]. The investigation of the origin of the change in slope in between the near and far SOL is beyond the scope of this work. We also remark that no ion temperature measurement is available, as is the case for most tokamaks. We invert the equations 3-4 to compute the loss factors f_q and f_{mom} from the profiles in Fig.5. The result is shown in Fig.6a for both experiments (dotted lines) and simulations (dashed (D) and solid (D+C) lines). The agreement between the total power loss f_q computed from experiments and simulations is satisfactory (except in the far SOL, where fitting issues arise for the experimental profiles due to the lack of TS measurements here), showing how most of the power is lost due to radiation from impurities close to the separatrix ($f_q > 1$), while power convection tends to be dominant in the far SOL ($f_q < 1$). While the application of the model to experimental data shows a sensible loss of momentum along the field lines ($f_{mom} \lesssim 0.75$), for the simulation we fall in the opposite situation $f_{mom} > 1$ everywhere except in the vicinity of the separatrix, leading to an apparent momentum gain. The latter is due to the assumption of the two point model $T_i = T_e$, in particular in the computation of the conservation of the total pressure (eq.(3)). In our simulations, this is not the case, as we imposed in the upstream SOL $T_i \geq T_e$ (Fig.5b,c). Furthermore, at the target the situation is reversed, being $T_i \leq T_e$. An apparent momentum gain was reported in Ref. [7] in ASDEX Upgrade for both experimental data and SOLPS simulations, and it was also attributed to the lack of T_i measurements in the experiments and to the $T_i = T_e$ assumption in the standard two-point model.

To overcome this discrepancy, we compare the simulation results with a two-fluid two point model. Indeed, in the SOL electrons and ions are usually thermally decoupled, the ion energy confinement $\tau_{||,i}$ being shorter than the ion-electron thermalization time $\tau_{th,ie}$ [8]. This is the case for our simulations as their ratio $R_{th} = \tau_{||,i}/\tau_{th,ie} \sim 10^{-31} n_u^2 L_{||}^{6/7}/q_{u,e}^{8/7} < 1$ ($R_{th} \sim 0.18$ and 0.3 for the D and D+C case, respectively). The thermal decoupling of electrons and ions allows us to separate the equation for heat conduction and conservation along the field line (eqs. (1,2)), allowing different heat conductivity for the two species, being $\kappa_{0,i} = \kappa_{0,e}\sqrt{m_e/m_i}$. We can separate the sheath transmission factor $\gamma_{sh} = 7$ into the contributions from ions and electrons, respectively $\gamma_{sh,i} = 2.5$ and $\gamma_{sh,e} = 4.5$, and we allow for independent power losses for ions and electrons. Finally, we include the ion temperature in the conservation of the total pressure. The two-fluid two point model reads then:

$$T_{u,s}^{7/2} = T_{t,s}^{7/2} + \frac{7 L_{||} f_{q,s} n_{t,s} c_s \gamma_{sh,s} T_{t,s}}{2\kappa_{0,s}} \tag{6}$$

$$2n_t(T_{t,e} + T_{t,i}) = f_{mom}(n_{u,e}T_{u,e} + n_{u,i}T_{u,i}) \tag{7}$$

the subscript $s = i, e$ for the two the plasma species, and $f_{q,s} \equiv f_{cond,s}/(1 - f_{power,s})$. We also allowed the electron and ion density to be different, to better compare with the case featuring impurities. We remark that, nevertheless, the approximation $n_e = n_i$ is valid within 10% in the SOL, and will not change significanlty the results. The application of the two-fluid two-point model to the simulation results in Fig.5 is shown in Fig.6b, where the electron and ion total power loss $f_{q,e}$ (blue), $f_{q,i}$ (green) and momentum loss f_{mom} (orange) are plotted for the D (dashed lines)

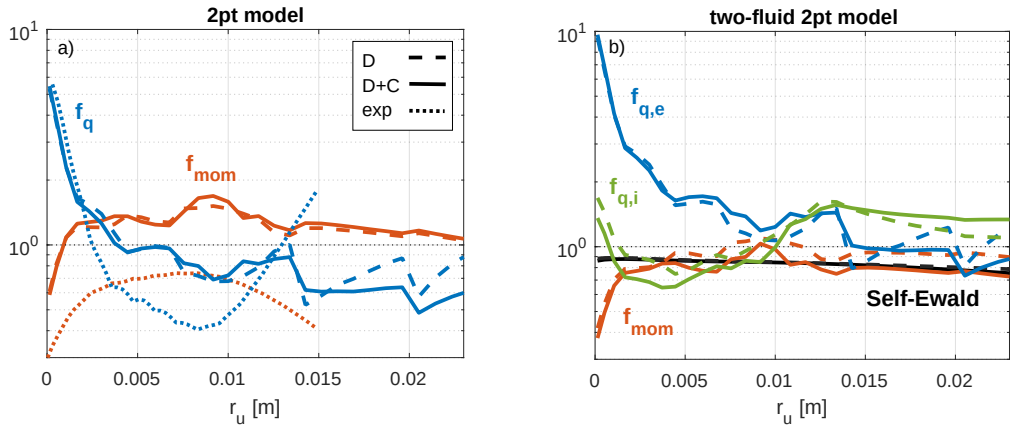

Figure 6: a) Radial profiles of total power loss f_q (blue) and momentum loss f_{mom} (orange), computed from experimental data (dotted lines) and simulation results (dashed (D) and solid (D+C) lines) using the standard two-point model (eqs. (3-4)). b) Radial profiles of electron and ion total power loss $f_{q,e}$ (blue), $f_{q,i}$ (green) and momentum loss f_{mom} (orange), computed from simulation results (dashed (D) and solid (D+C) lines) using the two-fluid two-point model (eqs. (6-7)), together with the momentum loss computed from the Self-Ewald model (eq.(8)), in black.

and D+C (solid lines) cases. We remark that the apparent momentum gain has now disappeared, being $f_{mom} \lesssim 1$ everywhere. Also, the computed f_{mom} shows a good agreement with the power loss predicted by the Self-Ewald model [18]

$$f_{mom,SE} = 2\left(\frac{\alpha}{\alpha+1}\right)^{(\alpha+1)/2} \tag{8}$$

where the coefficient $\alpha = \langle\sigma v\rangle_i/(\langle\sigma v\rangle_i + \langle\sigma v\rangle_m)$ is computed from the AMJUEL ionization and momentum loss rate coefficients, $\langle\sigma v\rangle_i$ and $\langle\sigma v\rangle_m$ respectively.

4 Conclusion

The inter-ELM phase of a TCV H-mode discharge featuring a long divertor leg has been modeled with the SolEdge2D-EIRENE code. The results from two simulations, the first one in pure deuterium and the second one including carbon impurities sputtered from the wall, are compared with experimental measurements from Thomson scattering, bolometry, divertor Langmuir probes and infrared thermography, finding an overall satisfactory agreement, improved in the case featuring impurities. Further modeling of TCV H-mode discharges featuring different divertor leg lengths is ongoing and will be reported in future works. The application of the standard two-point model to the simulation results would lead to an apparent momentum gain in the divertor, due to the hypotheses $T_i = T_e$, not satisfied here, similarly to what already reported in Ref. [7]. The application of a two-fluid two-point model, featuring thermally decoupled ions and electrons to the simulation results overcomes this discrepancy. This result points to the general need for reliable ion temperature measurements in the experiments and its consistent inclusion in the model for the correct interpretation of the results of both experiments and simulations.

Acknowledgments

This work was granted access to the HPC resources of CINES, under the allocation i2015056912 made by GENCI and to the HPC resources of Aix-Marseille University financed by the project Equip@Meso (ANR-10-EQPX-29-01). The project leading to this publication (TOP project) has received funding from Excellence Initiative of Aix-marseille University- A*MIDEX, a french "Investissements d'Avenir" programme. This work has been carried out within the framework of the EUROfusion Consortium and has received funding from the Euratom research and training programme 2014-2018 under grant agreement No 633053. The views and opinions expressed herein do not necessarily reflect those of the European Commission.

References

[1] S. Coda, J. Ahn, R. Albanese, S. Alberti, E. Alessi, S. Allan, H. Anand, G. Anastassiou, Y. Andrebe, C. Angioni, et al. **Overview of the TCV Tokamak Program: Scientific Progress and Facility Upgrades**. *Nuclear Fusion*, **57**:102011, 2017.

[2] A. Gallo, N. Fedorczak, S. Elmore, R. Maurizio, H. Reimerdes, C. Theiler, C. K. Tsui, J. A. Boedo, M. Faitsch, H. Bufferand, et al. **Impact of the plasma geometry on divertor power exhaust: experimental evidence from TCV and simulations with SolEdge2D and TOKAM3X**. *Plasma Physics and Controlled Fusion*, **60**:014007, 2017.

[3] R. Maurizio, S. Elmore, N. Fedorczak, A. Gallo, H. Reimerdes, B. Labit, C. Theiler, C.K. Tsui, W.A.J. Vijvers, The TCV Team and The MST1 Team. **Divertor power load studies for attached L-mode single-null plasmas in TCV**. *Nuclear Fusion*, **58**:016052, 2018.

[4] H. Bufferand, G. Ciraolo, Y. Marandet, J. Bucalossi, Ph. Ghendrih, J. Gunn, N. Mellet, P. Tamain, R. Leybros, N. Fedorczak, et al. **Numerical modelling for divertor design of the WEST device with a focus on plasmawall interactions**. *Nuclear Fusion*, **55**:053025, 2015.

[5] G. Ciraolo, H. Bufferand, J. Bucalossi, Ph. Ghendrih, P. Tamain, Y. Marandet, M. Valentinuzzi, J. Denis, N. Fedorczak, E. Hodille, N. Mellet, B. Pegourie, C. Grisolia, C. Bourdelle, E. Tsitrone, D. Galassi, R. Leybros, G. Giorgiani, E. Serre. **H-mode WEST tungsten divertor operation: deuterium and nitrogen seeded simulations with SOLEDGE2D-EIRENE**. *Nuclear Materials and Energy*, **12**:187–192, 2017.

[6] P.C. Stangeby. **The Plasma Boundary of Magnetic Fusion Devices** . *Institute of Physics Publishing Bristol and Philadelph*, 2000.

[7] I.Paradela Pereza, A.Scarabosio, M.Groth, M.Wischmeier, F.Reimold, ASDEXUpgrade Team. **SOL parallel momentum loss in ASDEX Upgrade and comparison with SOLPS**. *Nuclear Materials and Energy*, **12**:181–186, 2017.

[8] C.S. Pitcher and P.C. Stangeby. **Experimental divertor physics**. *Plasma Physics and Controlled Fusion*, **39**:779–930, 1993.

[9] V. Kotov and D. Reiter. **Two-point analysis of the numerical modelling of detached divertor plasmas**. *Plasma Physics and Controlled Fusion*, **51**:115002, 2009.

[10] J.-M. Moret, B.P. Duval, H.B. Le, S. Coda, F. Felici, H. Reimerdes. **Tokamak equilibrium reconstruction code LIUQE and its real time implementation**. *Fusion Engineering and Design*, **91**:1–15, 2015.

[11] O. Fevrier, C. Theiler, H. De Oliveira, B. Labit, N. Fedorczak, and A. Baillod. **Analysis of wall-embedded Langmuir probe signals in different cnditions on the Tokamak a Configuration Variable**. *Review of Scientific Instruments*, **89**:053502, 2018.

[12] F. D. Halpern and P. Ricci. **Velocity shear, turbulent saturation, and steep plasma gradients in the scrape-off layer of inner-wall limited tokamaks**. *Nuclear Fusion*, **57**:034001, 2017.

[13] F. Nespoli, B. Labit, I. Furno, J. Horacek, C.K. Tsui , J.A. Boedo, R. Maurizio, H. Reimerdes, C. Theiler, P. Ricci, F.D. Halpern, U. Sheikh, K. Verhaegh, R.A. Pitts, F. Militello, The EUROfusion MST1 Team and The TCV Team. **Understanding and suppressing the near Scrape-Off Layer heat flux feature in inboard-limited plasmas in TCV**. *Nuclear Fusion*, **57** :126029, 2017.

[14] J. Loizu, J. A. Morales, F. D. Halpern, P. Ricci, P. Paruta. **Scrape-off-layer current loops and floating potential in limited tokamak plasmas**. *Journal of Plasma Physics*, **83**:57583601, 2017.

[15] R.J. Groebner and T.N. Carlstrom. **Critical edge parameters for H-mode transition in DIII-D**. *Plasma Physics and Controlled Fusion*, **40**:053502, 1998.

[16] M. Kocan, R.A. Pitts, G. Arnoux, I. Balboa, P.C. de Vries, R. Dejarnac, I. Furno, R.J. Goldston, Y. Gribov, J. Horacek, et al. **Impact of a narrow limiter SOL heat flux channel on the ITER first wall panel shaping**. *Nuclear Fusion*, **55**:033019, 2015.

[17] F. Wagner. **A study of the perpendicular particle transport properties in the scrape-off layer of ASDEX**. *Nuclear Fusion*, 5:525, 1985.

[18] S.A. Self and H.N. Ewald. **Static Theory of a Discharge Column at Intermediate Pressures**. *The Physics of Fluids*, **9**:2486, 1966.